

A STUDY ON THE EFFECT OF NOZZLE GEOMETRICAL PARAMETERS ON SUPERSONIC COLD SPRAYING OF DROPLETS

Semih Akin, Puyuan Wu, Chandra Nath, Jun Chen, Martin Byung-Guk Jun*
 Purdue University, School of Mechanical Engineering, West Lafayette, IN, 47906, USA

ABSTRACT

Supersonic cold spraying of droplets containing functional nanomaterials is of particular interest in advanced thin-film coating, that enabling high-adhesion strength particle deposition. In this method, coating occurs when the particles are accelerated to supersonic velocities in a converging-diverging nozzle, and then impact onto a target surface. Here, the optimum design of the nozzle is essential to deal with low-inertia particles like droplets. In particular, nozzle geometrical parameters (i.e., throat diameter; exit diameter; divergent length) determine droplets' acceleration and deposition characteristics under supersonic flow conditions. To this end, we thoroughly investigate the influence of nozzle geometrical parameters on droplets acceleration by numerical modeling followed by experimental validation, and a case study on surface coating application. Two-phase flow modeling was used to predict droplets' behavior in continuous gas flow for different nozzle configurations. The results show that the nozzle expansion ratio - a function of throat and exit diameters - has a significant influence on droplet velocity, followed by divergent length. In particular, to correctly accelerate low-inertia liquid droplets, optimum nozzle expansion ratio for an axisymmetric convergent-divergent nozzle is found to be in a range of 1.5-2.5 for various sets of parameters, which is different than the recommended expansion ratio (i.e., 5-9) for cold spraying of micro-scale metal particles. The findings can help determine the ideal design of a supersonic nozzle to minimize turbulent velocity fluctuation and shock wave formation that in turn assist to effectively spray low-inertia particles like micro-scale droplets. Based on the simulation results, an optimal design of supersonic nozzle is selected and prototyped for the experimental studies. Numerical modeling results are validated by particle image velocimetry (PIV) measurements. Moreover, coating experiments confirm the adaptability of the optimized nozzle for supersonic cold spraying of droplets containing nanoparticles, which thereby has the potential for rapid production of advanced thin films.

Keywords: Supersonic spraying, cold spray, coating, numerical modeling, CFD, nanomaterial, thin film, PIV

NOMENCLATURE

Symbol	Description
A	Area
C_c	Cunningham slip correction factor
C_s	vapor concentration at the droplet surface
C_∞	vapor concentration of the bulk flow
d_c	Nozzle exit diameter
d_{th}	Nozzle throat diameter
D_m	Diffusion coefficient for species
e	Specific internal energy
\vec{F}	Force vector
\vec{F}_{Ba}	Basset force
\vec{F}_{Bu}	Buoyancy force
\vec{F}_D	Stokes drag force
\vec{F}_{Mag}	Magnus lift force
\vec{F}_{Pg}	Pressure gradient force
\vec{F}_{Saff}	Saffman lift force
\vec{F}_{VM}	Virtual mass force
g	Gravitational constant
h_c	Heat transfer coefficient
h_{fg}	Latent heat
\vec{J}	Mass diffusion flux in turbulent flow
k	Thermal conductivity
k_c	Mass transfer coefficient
L_{div}	Nozzle divergent length
Nu	Nusselt number
Pr	Prandtl Number
P	Fluid pressure
Re	Reynolds number
S_y	Source term of species
Greek letters	
ρ	Fluid density
ρ_p	particle density
μ_t	Turbulent viscosity
λ	Molecular mean free path
$\bar{\tau}$	Viscous stress tensor
Abbreviations	
CFD	Computational fluid dynamics
PIV	Particle image velocimetry
PET	Polyethylene terephthalate

* Corresponding author: mbgjun@purdue.edu

1. INTRODUCTION

Supersonic cold spray coating is an emerging technique for the deposition of micro-and nano-particles in a rapid and high-throughput manner. The scalability and the cost-effectiveness of this technique make it favorable for many applications such as solar cells, transparent conductive films, energy-storage materials, etc. [1]. In this technique, the particles are accelerated to supersonic velocities through a supersonic nozzle (*i.e.*, also known as convergent-divergent nozzle, or *de Laval* nozzle) using compressed gases, then the particles impact on a target surface, producing strong interfacial adhesion owing to the high-impact velocity of particles [1]. Herein, the supersonic nozzle is the backbone of the cold spraying process to accelerate the coating materials to desired velocities prior to impact by generating a supersonic jet. The design of a supersonic nozzle also determines the deposition efficacy of the coating process.

The typical coating materials of cold spray are mainly gas atomized spherical-shaped solid-state metal microparticles [2]. In recent years, many attempts have been made to optimally design of supersonic nozzles for spraying these important metal particles [3–9]. Li et al. [4] investigated the effect of nozzle geometry on particle acceleration in cold spraying process. Yin et al. [6] studied the effect of different nozzle cross-section shapes on gas flow and particle acceleration in cold spraying. Sova et al. [10,11] scaled down the conventional cold spray nozzles by developing a micronozzle for high-resolution cold spray deposition of aluminum powders. In these studies, the main focus was given on cold spraying of solid-state metal particles having a size range of 5–50 μm , and notable results regarding the nozzle design were reported to guide the researchers. Despite significant outputs, the conventional cold spraying method is limited for micron-scale metal particles, and it is not applicable for supersonic spraying of nanomaterials which are generally in colloidal suspension form. Seongpil et al. [1] modified the downstream injection of the conventional cold spray nozzles to be able to spray liquid-based nanomaterials (*i.e.*, suspension or colloid) from atomized droplets. Through this approach, promising results in nanotechnology have been achieved, and it has paved the way for state-of-the-art applications.

Most recently, our group systematically studied dispersion and deposition characteristics of micron-scale atomized ‘liquid’ droplets under supersonic flow conditions for nanocoating applications [12]. In that study, generalized parameter windows for supersonically spraying of droplets were presented to provide useful information for the researchers. The study, however, did not consider the effect of nozzle geometrical parameters on droplet flow behavior in a supersonic jet. Despite great promises, a critical need remains to understand the influence of nozzle geometrical parameters on droplets behavior under supersonic flow conditions. Understanding the effect of nozzle geometrical parameters on droplets velocity is vital to improving the efficacy of functional nano-coating from atomized droplets. These are integral to practical deployment of supersonic cold spray deposition in nanocoating and advanced thin-film technology.

To this end, the present work is devoted to studying the influence of nozzle geometrical parameters on droplets’ flow characteristics under supersonic spray conditions. This study addresses the effect of nozzle exit diameter (d_{ex}), nozzle throat diameter (d_{th}), and nozzle divergent length (L_{div}) on spray jet formation and droplets acceleration considering different droplet sizes in a range of 5–30 μm . The nozzle expansion ratio (*i.e.*, ratio of the areas of nozzle exit to throat, d_{ex}^2/d_{th}^2) was estimated from the corresponding nozzle exit and throat diameters to determine an optimum expansion ratio for an effective supersonic spraying process. Based on the numerical modeling results, the optimal design of the supersonic nozzle is achieved and prototyped. An experimental validation study and a case study on coating experiments using the optimized nozzle are then presented. The key research contribution of this work is to draw an insight of the nozzle design for supersonic spray deposition of low-inertia micro-scale droplets for functional nano-coating applications utilizing the droplets as the transport medium.

2. MATERIALS AND METHODS

Numerical simulations were performed by using commercial software (ANSYS-Fluent) to determine the flow characteristic of the continuous gas and discrete droplet phases. Air was used as the driving gas while water droplets were considered for the discrete phase due to comparable similarity of water (*i.e.*, density, viscosity) with most of the nanomaterial

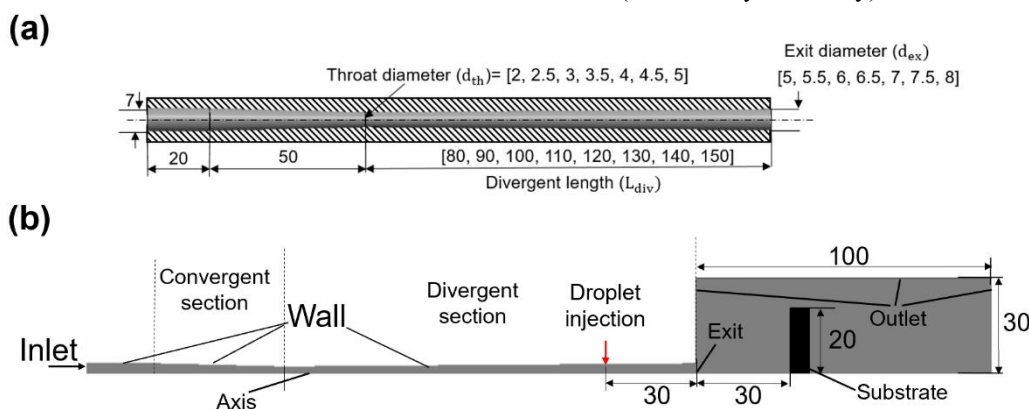


FIGURE 1. SCHEMATIC OF (a) SUPERSONIC NOZZLE, (b) COMPUTATIONAL DOMAIN AND BOUNDARIES (Scale: mm).

solutions [12]. The nozzle dimensions and boundary conditions of the computational domain are presented in Figures 1(a)-(b), respectively. The flow domain was discretized with the structured elements having 210,000 cells to obtain a grid-independent solution. The y^+ value (*i.e.*, non-dimensional distance from the wall of the first mesh node) was calculated as 29 for the discretized flow domain, which indicates a suitable selection where the turbulent flow is dominant [13]. A two-dimensional axisymmetric model was employed to decrease the computational time. A coupled discrete phase modeling (*i.e.*, Eulerian-Lagrangian approach) was used to track the droplets and investigate the droplets' acceleration for different nozzle geometrical configurations. A steady-state pressure-based solver was used considering compressibility effects. The realizable k - ϵ turbulence model with enhanced wall treatment was considered to model the turbulence effects [13].

The boundary conditions are listed in Table 1. To elaborate, gas pressure and temperature were defined as the inlet boundary. The whole side surface of the nozzle and the substrate were considered as adiabatic walls with no-slip boundary. In addition, the trap boundary condition was assigned to the nozzle walls and the substrate surface to capture the impinging droplets. The outlet pressure boundary condition was set to the atmospheric pressure (1 atm) at the nozzle exit and surroundings.

TABLE 1 BOUNDARY CONDITIONS.

Location	Pressure (P)	Velocity (u)	Temperature (T)
Nozzle inlet	Specified	$\partial u / \partial n = 0$	Specified
Nozzle walls	$\partial P / \partial n = 0$	0	$\partial T / \partial n = 0$
Symmetrical axis	$\partial P / \partial r = 0$	$\partial u / \partial r = 0$	$\partial T / \partial r = 0$
Surrounding atmosphere	Ambient condition	$\partial u / \partial n = 0$	$\partial T / \partial n = 0$

The governing equations of continuous gas phase for a steady compressible turbulent flow can be written as follows [13]:

Continuous phase (driving gas):

Continuity equation

$$\nabla \cdot (\rho \vec{u}) = S_m \quad (1)$$

Momentum equation

$$\nabla \cdot (\rho \vec{u} \vec{u}) = -\nabla p + \nabla \cdot \bar{\tau} + S_f \quad (2)$$

Energy equation

$$\nabla \cdot (\rho e \vec{u}) = -p \nabla \cdot \vec{u} + \nabla \cdot (k \nabla T) + \Phi + S_H \quad (3)$$

Transport equations

$$\nabla \cdot (\rho \vec{u} Y) = -\nabla \cdot \vec{J} + S_Y \quad (4)$$

$$\vec{J} = -\left(\rho D_m + \frac{\mu_t}{Sc_t}\right) \nabla Y \quad (5)$$

Equation of state

$$P = \rho RT \quad (6)$$

where ρ is the gas density (kg/m^3), \vec{u} is the velocity (m/s), $\bar{\tau}$ is the viscous stress tensor, p is the static pressure (Pa), e is the specific internal energy (J/kg), k is the thermal conductivity ($\text{W}/(\text{m}\cdot\text{K})$), T is the temperature (T), Y is the local mass fraction of the species, \vec{J} is the mass diffusion flux ($\text{kg}/(\text{m}^2\cdot\text{s})$) in turbulent flow, and μ_t is the turbulent viscosity ($\text{kg}/\text{m}\cdot\text{s}$). S_m , S_f , S_H , S_Y are the source terms to include the droplet evaporating species, droplet forces, and evaporation energy from the discrete phase, D_m is the diffusion coefficient for species in the mixture, and Sc_t is the Schmidt number. In the present study, the species are the water vapor in the air.

Discrete phase (droplets):

The Lagrangian approach was used to track the droplets inside the continuous phase flow and to consider the interaction between the phases. The droplets velocity and trajectory were calculated by using Newton's second law as given in Eq.7, where \vec{u}_d is the droplet velocity (m/s), ρ_d is the droplet density (kg/m^3), and $\sum \vec{F}$ is the sum of hydrodynamic forces; \vec{F}_D is the Stokes drag force, \vec{F}_{Ba} is the Basset force, \vec{F}_{VM} is the virtual mass force, \vec{F}_{Pg} is the pressure gradient force, \vec{F}_{Bu} is the buoyancy force, \vec{F}_{Saff} is the Saffman lift force, and \vec{F}_{Mag} is the Magnus lift force in the unit of Newton ($\text{kg}\cdot\text{m}/\text{s}^2$). In this study, the drag force, Brownian force, and Saffman lift force were considered for micro-scale droplets. The Cunningham slip correction factor (C_c) given in Eq.8 was also used to correct the Stoke's drag flow for micro-scale particles where d_p is the particle diameter (m), ρ_p is the particle density (kg/m^3), and λ is the molecular mean free path (m) [14].

To consider the heat transfer between the gas phase and the droplets, the conservation of energy equation given in Eq.9 was considered where A is the surface area of the droplet (m^2), h_{fg} is the latent heat (J/kg), h_c is the heat transfer coefficient ($\text{W}/(\text{m}^2\cdot\text{K})$). The radiative heat transfer was neglected since the driving gas temperature is low in the divergent section of the nozzle due to the rapid gas expansion.

The evaporation rate of the droplet was calculated using Eq.10, where k_c is the mass transfer coefficient ($(\text{mol}/\text{s})/(\text{m}^2\cdot\text{mol}/\text{m}^3)$), C_s is the vapor concentration (g/m^3) at the droplet surface, C_∞ is the vapor concentration of the flow (g/m^3). In addition, the Discrete Random Walk model [13] was employed to analyze the turbulent dispersion of the droplets in the spray flow and effects on droplets trajectory by considering the instantaneous fluctuation of driving gas velocity.

$$m_d \frac{d\vec{u}_d}{dt} = \sum \vec{F} = \vec{F}_D + \vec{F}_{Ba} + \vec{F}_{VM} + \vec{F}_{Pg} + \vec{F}_{Bu} + \vec{F}_{Saff} + \vec{F}_{Mag} \quad (7)$$

$$C_c = 1 + \frac{2\lambda}{d_p} \left[1.257 + 0.4 \exp\left(-\frac{1.1d_p}{2\lambda}\right) \right] \quad (8)$$

$$m_p c_p \frac{dT_p}{dt} = h_c A (T - T_p) + h_{fg} \frac{dm_p}{dt} \quad (9)$$

$$\frac{dm_p}{dt} = -Ak_c (C_s - C_\infty) \quad (10)$$

3. SIMULATION RESULTS AND DISCUSSIONS

An optimal design of a supersonic nozzle should be performed for a fixed inlet gas pressure, and then the geometrical parameters (*e.g.*, nozzle expansion ratio, divergent length) should be determined for that pressure value to achieve the maximum particle impact velocity [15]. Given that information, we study the influence of nozzle geometrical parameters on droplets acceleration at a driving gas pressure of 0.7 MPa to be consistent with our previous study [12]. We also test the nozzle expansion ratio for a different inlet gas pressure (*i.e.*, 0.5 MPa). The parameters involved in computational fluid dynamics (CFD) simulations are listed in Table 2.

TABLE 2 PARAMETERS INVOLVED IN SIMULATIONS.

Throat diameter, d_{th} , (mm)	2, 2.5, 3, 3.5, 4, 4.5, 5
Exit diameter, d_{ex} , (mm)	5, 5.5, 6, 6.5, 7, 7.5, 8
Divergent length, L_{div} , (mm)	110, 120, 130, 140
Droplet diameter (μm)	5, 10, 15, 20, 25, 30
Driving gas pressure (MPa)	0.5, 0.7
Driving gas temperature (K)	300 (Room temperature)

3.1 Effect of nozzle throat diameter on droplet velocity

Figures 2(a)-(b) show the effect of the nozzle throat diameter on upon-impact velocity of droplets considering two different nozzle exit diameters (*i.e.*, $d_{ex} = 6.5$ and 5.5 mm), respectively, for different sizes of droplets. The gas inlet pressure and nozzle divergent length are set to be constant at 0.7 MPa and 130 mm, respectively. One important finding is that there exists a maximum droplet velocity for a certain nozzle configuration for any droplet sizes that are considered. The highest droplet velocity of 471 m/s was obtained for the throat diameter of 4.5 mm and exit diameter of 6.5 mm (Figure 2a) as compared to the highest velocity of 465 m/s for the combination of 3.8 mm throat and 5.5 mm exit diameters (Figure 2b).

Another important finding in Figures 2(a)-(b) is that droplets experience a much lower impact velocity for the throat diameters of 2, 2.5, and 3 mm as compared to larger throat diameters. It is likely attributed to severe normal shock waves formation inside and outside of the nozzle (see Figure 3a). In particular, the nozzles with smaller throat diameters (*i.e.*, 2, 2.5, and 3 mm) create over-expanded spray jet, resulting in lower droplets' impact velocities. The shock waves start to develop inside the nozzle for the over-expanded jet, and eventually decelerate the gas velocity at the nozzle exit (see Figure 3a for $d_{th}=2, 2.5,$ and 3 mm). Conversely, for the under-expanded jet flow (Figure 3a for $d_{th} = 3.5, 4,$ and 5 mm), the gas velocity is higher than over-expanded nozzle configuration at the nozzle exit, which explains the higher droplets' impact velocity for these nozzle geometries (see Figure 2(a)-(b)). Moreover, droplets at $\leq 10 \mu\text{m}$ are more susceptible to normal shock waves, experiencing significantly

lower velocities for over-expanded spray flow (see Figures 2(a)-(b)) for $d_{th}=2, 2.5,$ and 3). These results suggest that a nozzle having over-expanded jet flow is not a suitable choice for the supersonic spraying of low-inertia particles like droplets.

The highest droplet velocity was obtained at 4.5 mm for the correctly expanded nozzle configuration (enclosed image in Figure 3a). It shows minimum shock wave formation inside and outside of the nozzle for the correctly expanded flow. It implies that shock waves have a critical impact on the acceleration of micro-scale low-inertia droplets in the supersonic spraying process, which can be controlled by the throat diameter. The results are consistent with the literature concluding that undesirable shear layers, expansion fan, and shock waves form if the nozzle is not designed in a correctly-expanded manner [9].

3.2 Effect of nozzle exit diameter on droplet velocity

Figures 2(c)-(d) show the influence of nozzle exit diameter on droplets' impact velocity for different throat diameters. It is observed that nozzle exit diameter is as not critical as throat diameter for droplet acceleration since the rapid expansion of the gas starts from the throat section and develops through the divergent section. The maximum droplet velocity was obtained for the nozzle having $d_{ex} = 6.5$ mm when $d_{th} = 4.5$ mm (Figure 2c) and $d_{ex} = 5$ mm when $d_{th} = 3.5$ mm (Figure 2d).

Another important finding from Figures 2(a)-(d) is that droplets' size also significantly influences the droplet velocity. A decrease in droplet diameter leads to higher impact velocities, particularly for the droplet diameter less than 15 μm . Conversely, the increase in droplet velocity for the larger droplets (*i.e.* $\geq 15 \mu\text{m}$) is not as remarkable as smaller droplets, which is likely attributed to the high inertia of larger droplets. The traditional cold spray feedstock powders also follow a similar flow behavior, having a decreasing impact velocity for larger droplets [16,17]. These results reveal that the smaller droplets could be preferred if there is a need for higher droplets impact velocity in cold spraying process.

3.3 Effect of nozzle expansion ratio on droplet velocity

The nozzle expansion ratio (*i.e.*, ratio of the cross-sectional areas of nozzle exit to throat, d_{ex}^2/d_{th}^2), was calculated to investigate the combined effect of nozzle throat and exit diameters on droplets velocity. As seen in Figures 2(e)-(f), for any droplet size, there exists an optimum nozzle expansion ratio at certain inlet gas pressure to effectively accelerate low-inertia droplets to supersonic velocities. The highest velocity of droplets was obtained for the nozzle expansion ratio of 2.086 and 2.04 at inlet gas pressures of 0.7 MPa and 0.5 MPa, respectively (see Figures 2(e)-(f)). Both results correspond to the flow with minimum shock wave formation and turbulent velocity fluctuation inside and outside of the nozzle (Figures 3(a)-(b)).

Previous studies on traditional cold spraying reported that the typical value of nozzle expansion ratio for supersonically spraying of micro-scale solid-state particles should be in a range

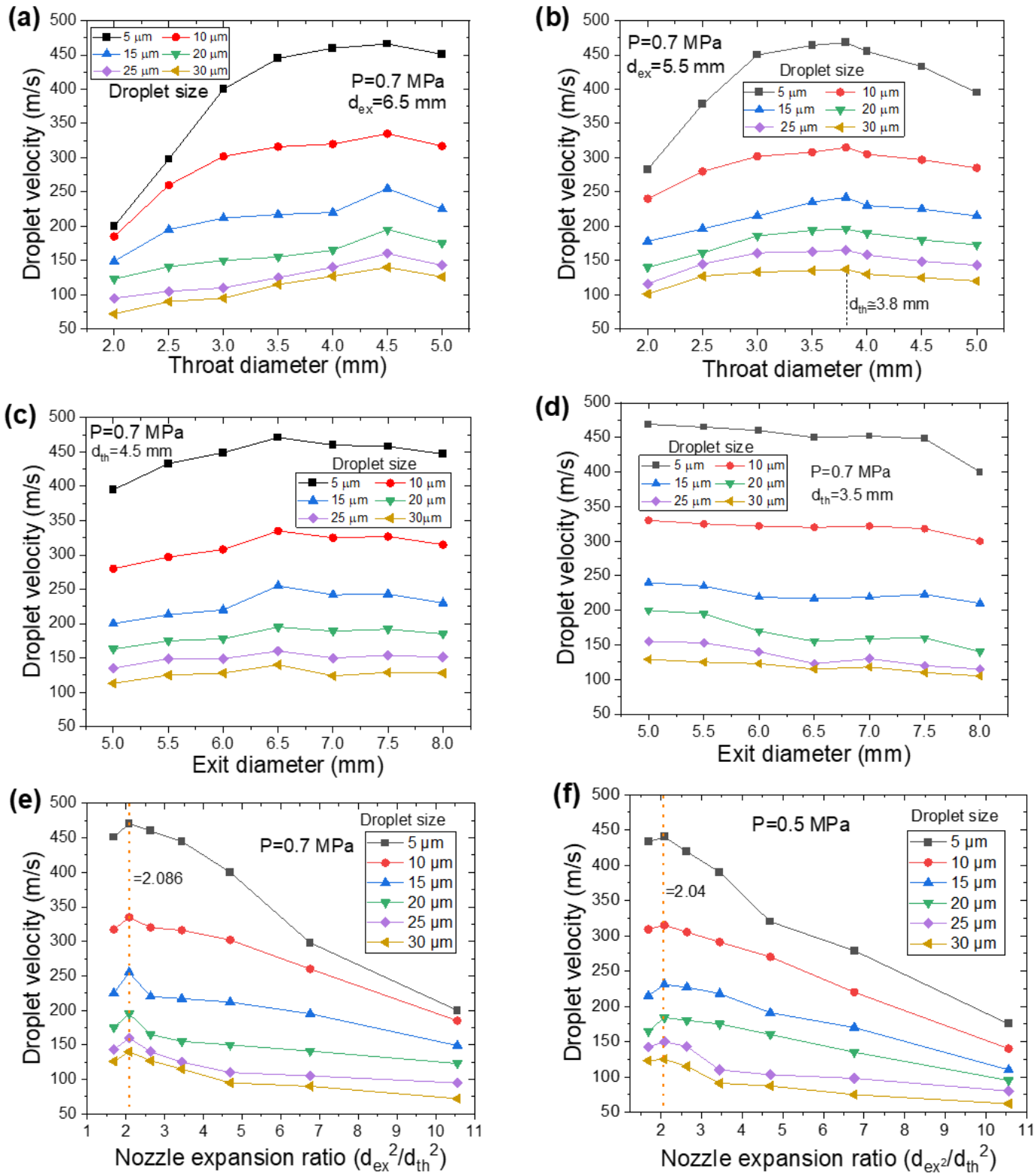


FIGURE 2. EFFECT OF NOZZLE THROAT DIAMETER ON DROPLET VELOCITY; (a) P=0.7 MPa, $d_{ex}=6.5$ mm, (b) P=0.7 MPa, $d_{ex}=5.5$ mm; EFFECT OF NOZZLE EXIT DIAMETER ON DROPLET VELOCITY; (c) P=0.7 MPa, $d_{th}=4.5$ mm, (d) P=0.7 MPa, $d_{th}=3.5$ mm; EFFECT OF NOZZLE EXPANSION RATIO ON DROPLET VELOCITY; (e) P=0.7 MPa, (f) 0.5 MPa; (Temperature= 300K and $L_{div}=130$ mm for all analyses).

of 5 and 9 to have the Mach number of 2-3.5 at the nozzle exit [18]. In the present study, however, we interestingly observed that the optimum nozzle expansion ratio for supersonically spraying of low-inertia micro-scale liquid droplets is in a range of 1.5-2.5, which is different than the suggested value of nozzle expansion ratio in Ref [18] for traditional cold spray feedstock material of micro-scale metal powders.

This study reveals that micro-scale liquid droplets behave differently under supersonic flow conditions as compared to typical feedstock materials (*i.e.*, metal particles) in cold spraying process. As a noteworthy result, micron-scale droplets do not obey the recommendations on optimal expansion ratio of cold spray nozzle design suggested in the literature for cold spraying of metal particles [18,19]. Moreover, droplets are more susceptible to turbulent velocity fluctuation and normal shock-wave formation compared to metal particles due to droplets' lower inertia, so that geometrical parameters should be carefully selected for effective supersonic spraying of droplets containing functional nanomaterials. Taken together, the ideal design of a supersonic nozzle to deal with low-inertia particles like droplets should possess correctly-expanded flow with minimum shock wave formation and turbulent velocity fluctuation, having an optimal expansion ratio at a certain driving gas pressure.

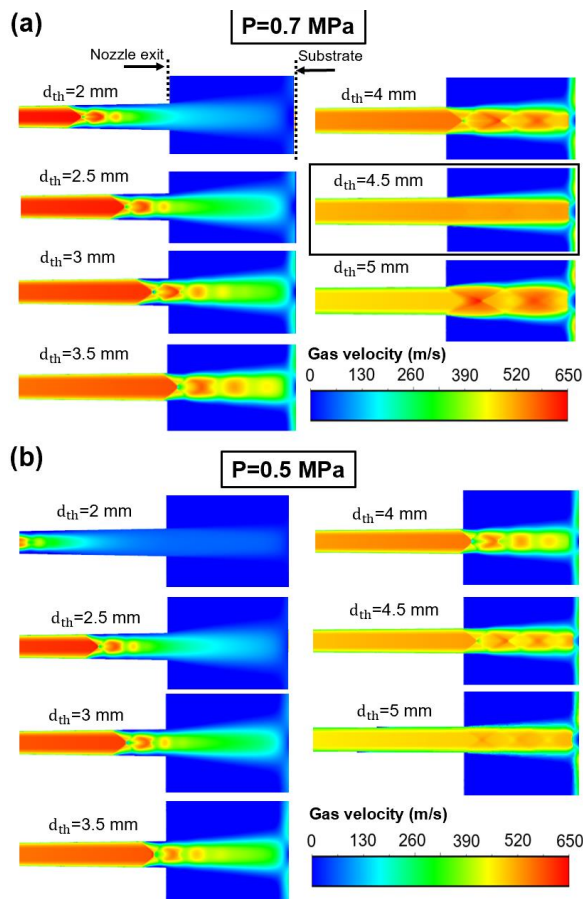


FIGURE 3. CONTOURS OF DRIVING GAS VELOCITY FOR DIFFERENT NOZZLE THROAT DIAMETERS AT (a) $P=0.7$ MPa, (b) 0.5 MPa where $L_{div}=130$ mm and $d_{ex}=6.5$ mm.

3.4 Effect of divergent length on droplet velocity

The previous studies on supersonic nozzle design for cold spraying of metal particles reported that nozzle divergent length has an important influence on micron-scale particle acceleration [4]. Especially, the divergent length should be long enough to provide an ideal accelerating path for the particles in the gas flow [18]. However, a very high value of divergent length leads to a drop in gas velocity due to the boundary layer growing on the nozzle walls [18]. Thus, the ratio between the divergent length and nozzle exit diameter (L_{div}/d_{ex}) determines the convenient acceleration of the particles [18]. In particular, the literature suggests that the typical value of L_{div}/d_{ex} for a supersonic spray nozzle for suitable particle acceleration should be in a range of 15-20 [18,20].

In this study, based on the information stated above, various divergent lengths (*i.e.*, 110, 120, 130, 140 mm) were selected to investigate the effect of divergent length on droplet acceleration by keeping the nozzle exit diameter, d_{ex} , constant as 6.5 mm. As seen in Figure 4, shorter divergent lengths (*i.e.*, $L_{div} = 110$ and 120 mm) result in lower droplet velocities. This is attributed to the shorter/insufficient acceleration path of the droplets in the supersonic section (*i.e.*, diverging section) of the nozzle. The maximum droplets velocities were obtained for the nozzle having a divergent length of 130 mm. For this nozzle configuration, the ratio of L_{div}/d_{ex} is estimated to be 20, which is consistent with the studies on cold spraying of micro-scale metal particles [18,20]. Further increase in divergent length (*i.e.*, $L_{div}=140$) leads to a relative decrease in droplet velocity, which could be attributed to the boundary layer growing (*i.e.*, friction) phenomenon on the nozzle walls [18]. Thus, it can be concluded that supersonically spraying of micro-scale droplets obeys the recommendations on divergent length selection for traditional cold spray feedstock of micro-scale metal particles.

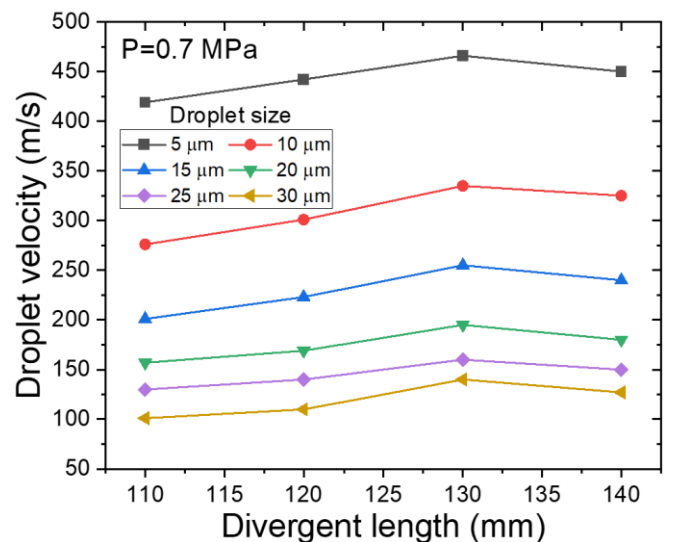


FIGURE 4. EFFECT OF NOZZLE DIVERGENT LENGTH ON DROPLET VELOCITY ($d_{th}=4.5$ mm and $d_{ex}=6.5$ mm).

4. EXPERIMENTAL CORRELATION

4.1 Experimental details

Based on the numerical simulation results, the optimum design of the supersonic nozzle was determined for an inlet pressure of 0.7 MPa and then developed a prototype as shown in Figure 5a. An atomization-assisted supersonic spray system, as presented in Figure 5b, was also constructed for Particle Image Velocimetry (PIV) measurements and coating experiments to justify the numerical modeling results and test the nozzle performance. The spray setup consists of two separate modules of atomization unit and supersonic nozzle (Figure 5b). In spraying experiments, first, nanomaterial solution is atomized into micro-scale droplets using an atomization unit. Next, the atomized droplets are carried into the nozzle injection port by a low-velocity carrier gas flow. Lastly, the central high-pressure gas flow accelerates the droplets to supersonic velocities and focuses the droplets onto the target surface.

The PIV technique was used to capture the velocity distribution of the sprayed droplets at the nozzle exit. Figure 5c illustrates the PIV setup, which consists of a dual Nd:YAG pulse laser (wavelength 532 nm, pulse length of 6 nanoseconds (ns), maximum energy of 200 mJ per pulse), a group of optical lenses,

and a charge-coupled device (CCD) camera (1,600×1,200 pixels). In PIV measurements, two laser pulses from the laser were spanned into a light sheet by using the optical lenses to illuminate the center plane of the spray flow field with a time interval of 1 ns.

The CCD camera recorded a total of 2,000 double-exposed images to calculate the droplets velocity. The velocity vectors of droplets were then calculated and plotted for comparison with numerical modeling results. A clear PIV image of the sprayed droplet stream can be seen in see Figure 6a. Further details regarding the PIV setup can be found in our previous study [12].

Surface coating experiments were also performed to show the utility of the optimally designed nozzle for coating applications. In this regard, an acrylic white paint solution (*i.e.*, consisting of well-dispersed titanium dioxide (TiO₂) nanoparticles in deionized water) was used to visualize the resultant coatings. The prepared solution was then atomized into fine droplets and sprayed onto a polymer substrate (*i.e.*, polyethylene terephthalate (PET)). The width of the coatings was predicted from the CFD simulations by capturing the trajectories of the impinging droplets. The results were then compared with the actual width of single-pass coatings obtained from the coating experiments using the spray setup shown in Figure 6b.

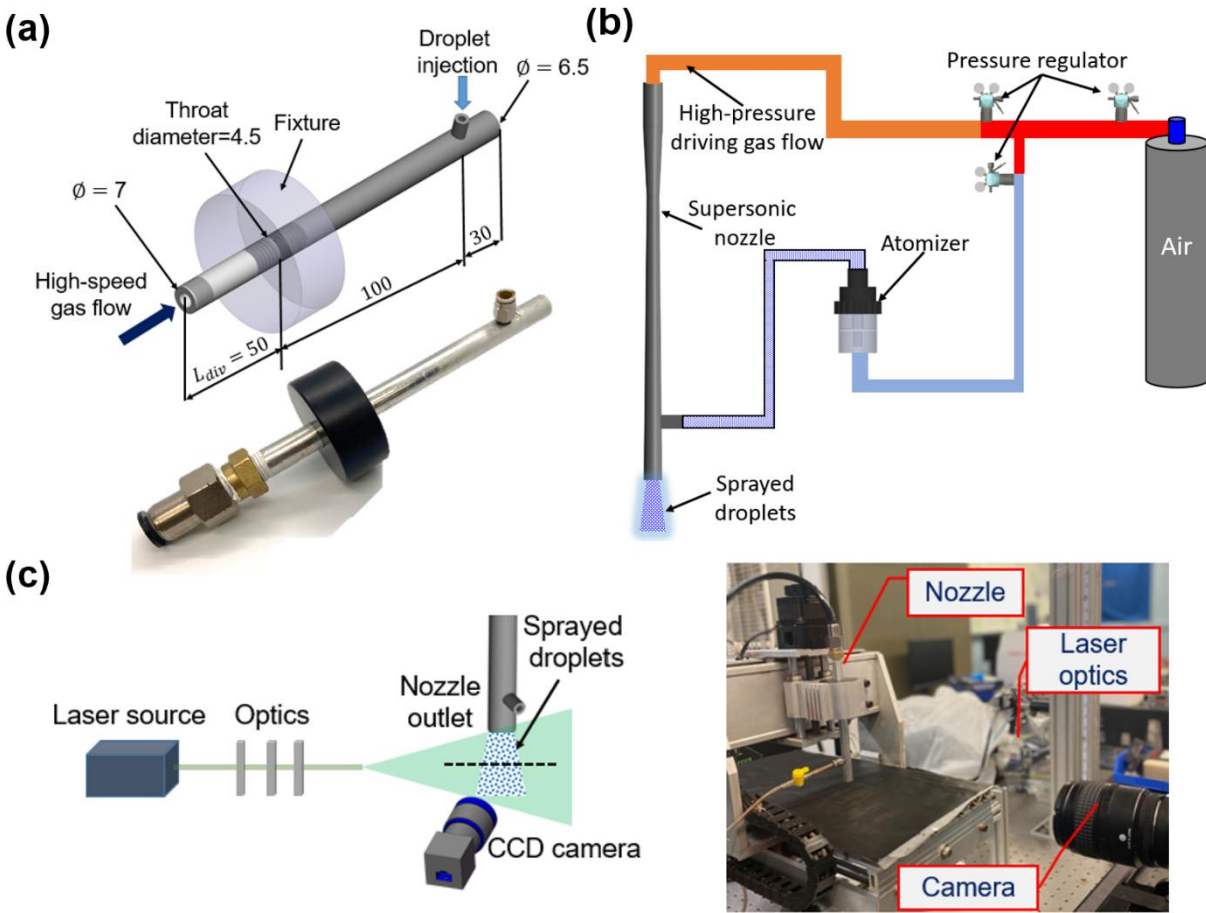


FIGURE 5. (a) OPTIMIZED SUPERSONIC NOZZLE, (b) SPRAY SETUP, (c) PIV SETUP (Scale in mm).

4.2 Experimental results and discussions

In the numerical simulations under this section, a droplet stream having the Rosin-Rammler size distribution was injected into the nozzle divergent section, and trajectories of the droplets were then tracked. The Rosin-Rammler size distribution as given in Eq.11 [13];

$$Y_d = e^{-(d/\bar{d})^n} \quad (11)$$

where, d is the droplet diameter, \bar{d} is the mean droplet diameter, n is the size distribution parameter, and Y_d is the mass fraction of droplets. The size distribution parameters previously stated were applied to the model by considering the atomizer's technical specifications, which can be found in Ref [21]. The simulation results were then compared with the PIV-measured velocity data followed by the coating experiments.

Figure 6a shows the PIV measured droplet velocity vector field from nozzle exit to the downstream of 28 mm (*i.e.*, 2 mm right before the impingement). Figure 6b presents the droplets' velocity trajectories at the nozzle exit obtained from the CFD simulations. Both CFD and PIV results show that the droplets are successfully accelerated to supersonic velocity using the optimally designed nozzle. Moreover, the CFD results of droplets velocity distribution are comparable to the PIV data, showing comparable spray morphology.

Figure 6c compares the CFD results with PIV measured averaged velocity along the radial direction of the nozzle exit for different downstream distances. Both simulation results and PIV measurements show a similar trend in droplet velocity. However, the numerical simulations predicted the droplets velocity higher than the PIV results. This can be attributed to the absence of a more precise droplet injection port in the computational flow domain and two-dimensional axisymmetric flow assumption in modeling. Taken together, the numerical simulations agree well with the experimental PIV measurements showing similar trends for velocity distribution of the droplets at the nozzle exit.

The coating experiments were also performed to further test the numerical modeling and optimized nozzle for actual spray coating scenarios. The coating experiments were performed using a 3-axis computer numerical control (CNC) stage to precisely control the spraying process. The nozzle transverse speed was set to 20 mm/min and one-pass spray coating was applied for different nozzle stand-off distances (SoD) (*i.e.*, spray distances). The coating results were then compared with the results obtained from numerical simulations.

Figure 7a shows the droplet trajectories for the half-portion of the nozzle for different droplet sizes acquired from numerical simulations. Figure 7b illustrates the experimental resultant coatings on the substrate at different spray distances. The main objective of Figure 7 is to compare the numerical modeling results with coating experiments in terms of coating width. As such, the sprayed droplets are tracked via numerical modeling, and the coating width was then predicted from impingement trajectories of the droplets on the target surface for each spray distance.

As seen in Figure 7, an increase in spray distance prompts the droplet dispersion onto the substrate, resulting in a lower spray resolution. The high dispersion characteristic of droplets onto the substrate surface for a longer spray distance is mainly responsible for this phenomenon. Another significant finding is that larger droplets better focus near the axis of the nozzle (see Figure 7a), leading to a thicker deposition at the central region of the coating as shown in Figure 7b. A possible reason for this could be the agglomeration of droplets in the nozzle after their injection. A CCD camera image in Figure 8a reveals that the droplets locally agglomerate at the central region of the nozzle during spraying. As such, the droplets form larger sizes at the near central region of the nozzle, leading to a thicker deposition on the central region of the resultant coating. The coating intensity, however, gradually decreases toward the outer region of the nozzle axis. The reason for this is the impingement of smaller droplets onto the outer side of the nozzle axis due to the susceptible nature of smaller droplets in the turbulent flow.

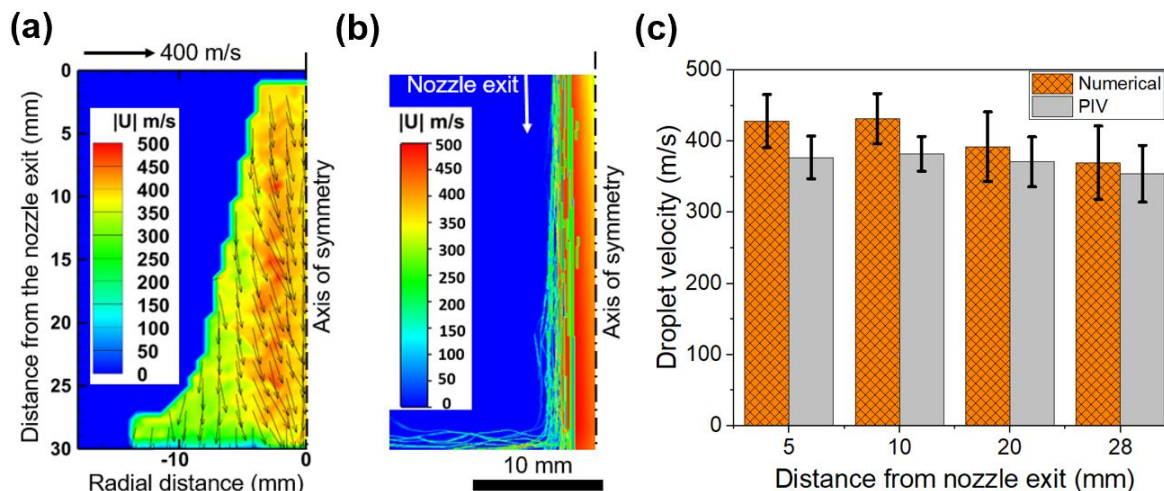


FIGURE 6. (a) PIV-MEASURED VELOCITY OF DROPLETS, (b) VELOCITY CONTOUR OF DROPLETS PREDICTED BY NUMERICAL SIMULATIONS, (c) COMPARISON OF PIV AND NUMERICAL RESULTS.

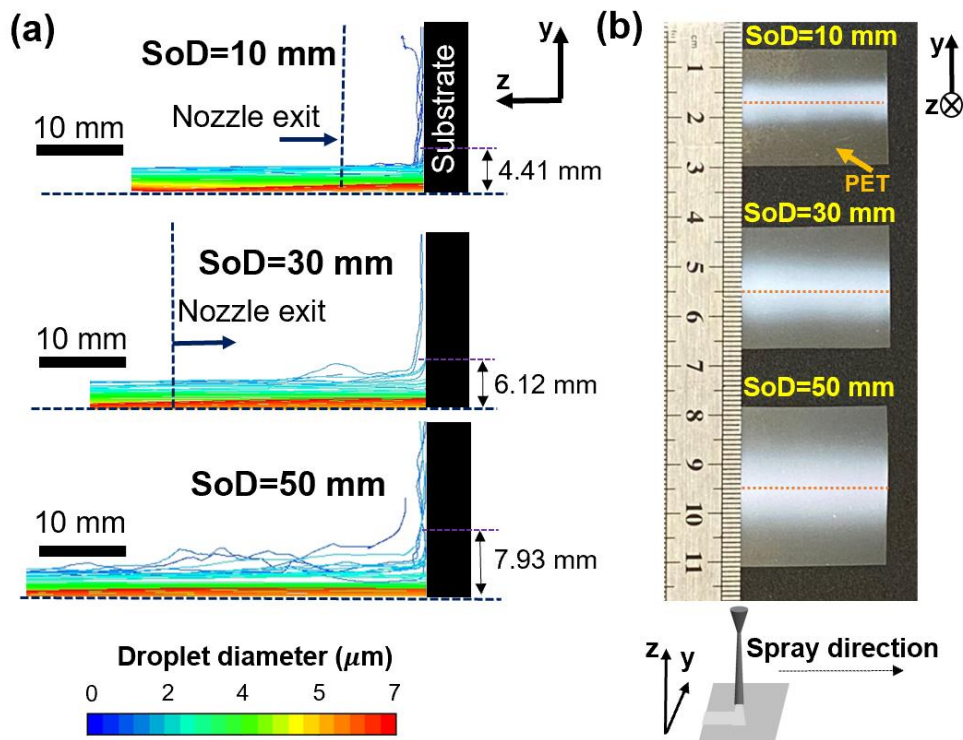


FIGURE 7. (a) DROPLET TRAJECTORIES FOR DIFFERENT SODs, (b) THE RESULTS OF COATING EXPERIMENTS.

Lastly, the numerical simulations and coating experiment results were compared in terms of coating width. Here, the coating width was predicted from numerical simulations by considering the trajectories of the impinging droplets onto the substrate surface in the radial direction. The width of the impinging droplet stream was calculated for the half-portion of the nozzle (see Figure 7a), and then the obtained value was doubled (i.e., multiplied by two) due to axis-symmetry to predict the actual spray width. In the coating experiments (see Figure 7b), the coating widths were measured from five different regions of the coating. The calculated values were then averaged to compare the experimental results with numerical simulations.

Figure 8b shows the comparison of numerical simulation results with the coating experiments. Both results follow a similar trend and show comparable results for spray width. The deviation in coating width increases as the spray distance (SoD) increases. It is attributed to the falling gas velocity at higher spray distances due to the negative drag force, resulting in more particle dispersion onto the target surface [22]. This analysis reveals that numerical modeling can be successfully used to predict the micro-scale droplets' dispersion and deposition behavior in supersonic flow conditions. Moreover, the experimental results suggest that the optimally designed supersonic nozzle and the spray system described in the present study could be successfully used to deposit the nanomaterials by utilizing droplets as the transport medium. In particular, the spray system has the potential for supersonic deposition of liquid-solution-based functional nanomaterials (e.g., colloids and suspensions), which are challenging to deposit these important materials onto surfaces due to their low inertia.

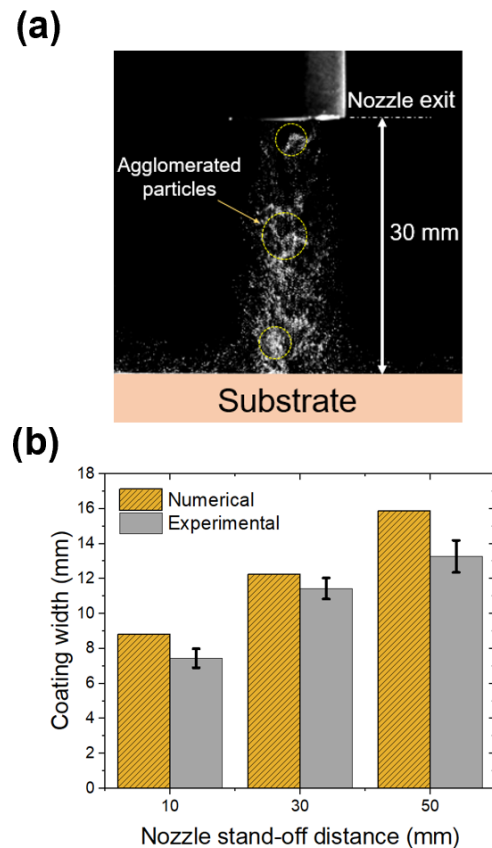


FIGURE 8. (a) A CCD CAMERA IMAGE OF JET STREAM AT SoD=30mm, (b) COMPARISON OF COATINGS WIDTHS.

5. CONCLUSION

In this study, the effect of nozzle geometrical parameters on supersonically spraying of micro-scale droplets was investigated by numerical modeling. A discrete phase (*i.e.*, *Eulerian-Lagrangian* approach) turbulent flow modeling was used to characterize the nozzle geometrical parameters for cold spraying of droplets. Based on the numerical modeling results, the optimal design of the supersonic nozzle was determined and prototyped. An atomization-assisted spray system was constructed for model validation and spray coating experiments. Numerical modeling results were validated by PIV measurements. The following conclusion can be drawn from the present study:

- Computational fluid dynamics (CFD) simulations revealed that nozzle expansion ratio (d_{ex}^2/d_{th}^2) is the main factor affecting droplets acceleration under supersonic flow conditions, followed by the divergent length.
- Micro-scale low-inertia droplets are much susceptible to turbulent velocity fluctuation of the continuous gas flow and shock wave forming inside and outside of the nozzle.
- There exists an optimum nozzle expansion ratio for a set of nozzle parameters with the main influence of throat diameter and inlet gas pressure to effectively spray the droplets by mitigating the shock wave formation at the nozzle exit. This statement is true for any droplet size.
- As a noteworthy result, the optimum nozzle expansion ratio for supersonic spraying of low-inertia micron-scale droplets differs from the expansion ratio recommended in the literature for cold spraying of metal particles.
- To correctly accelerate liquid droplets, the optimum nozzle expansion ratio for an axisymmetric supersonic nozzle was found to be in a range of 1.5-2.5.
- The ideal design of a supersonic nozzle for spray deposition of low-inertia particles (*e.g.*, micron-scale droplets) should possess minimum shock wave formation and optimal expansion ratio at a specific inlet gas pressure.
- The coating experiments confirmed the adaptability of the optimized nozzle for supersonic spray deposition of droplets containing functional nanoparticles, thereby indicating the potential for rapid production of advanced thin films.
- Despite its advantages, one possible drawback of the constructed spray system could be its limitation for the deposition of high-viscous nanoparticle solutions due to their atomization difficulty.
- As future work, the authors will test the developed spray system for various operating parameters and nanomaterial solutions (*i.e.*, having different densities and viscosity) to establish a spray deposition window for nanocoating applications by minimizing trial and error processes. That would help to pragmatic deployment of supersonic cold spraying technology in advanced thin-film production in a rapid, scalable, and high-throughput manner.

REFERENCES

- [1] An, S., Joshi, B., Yarin, A. L., Swihart, M. T., and Yoon, S. S., 2020, "Supersonic Cold Spraying for Energy and Environmental Applications: One-Step Scalable Coating Technology for Advanced Micro- and Nanotextured Materials," *Adv. Mater.*, **32**(2), p. 1905028.
- [2] Yin, S., Cavaliere, P., Aldwell, B., Jenkins, R., Liao, H., Li, W., and Lupoi, R., 2018, "Cold Spray Additive Manufacturing and Repair: Fundamentals and Applications," *Addit. Manuf.*, **21**(April), pp. 628–650.
- [3] Li, W. Y., and Li, C. J., 2005, "Optimal Design of a Novel Cold Spray Gun Nozzle at a Limited Space," *J. Therm. Spray Technol.*, **14**(3), pp. 391–396.
- [4] Li, W. Y., Liao, H., Douchy, G., and Coddet, C., 2007, "Optimal Design of a Cold Spray Nozzle by Numerical Analysis of Particle Velocity and Experimental Validation with 316L Stainless Steel Powder," *Mater. Des.*, **28**(7), pp. 2129–2137.
- [5] Li, W. Y., Liao, H., Wang, H. T., Li, C. J., Zhang, G., and Coddet, C., 2006, "Optimal Design of a Convergent-Barrel Cold Spray Nozzle by Numerical Method," *Appl. Surf. Sci.*, **253**(2), pp. 708–713.
- [6] Yin, S., Wang, X. fang, and Li, W. ya, 2011, "Computational Analysis of the Effect of Nozzle Cross-Section Shape on Gas Flow and Particle Acceleration in Cold Spraying," *Surf. Coatings Technol.*, **205**(8–9), pp. 2970–2977.
- [7] Varadaraajan, V., and Mohanty, P., 2017, "Design and Optimization of Rectangular Cold Spray Nozzle: Radial Injection Angle, Expansion Ratio and Traverse Speed," *Surf. Coatings Technol.*, **316**, pp. 246–254.
- [8] Grujicic, M., Tong, C., DeRosset, W. S., and Helfritsch, D., 2003, "Flow Analysis and Nozzle-Shape Optimization for the Cold-Gas Dynamic-Spray Process," *Proc. Inst. Mech. Eng. Part B J. Eng. Manuf.*, **217**(11), pp. 1603–1613.
- [9] Lee, M. W., Park, J. J., Kim, D. Y., Yoon, S. S., Kim, H. Y., Kim, D. H., James, S. C., Chandra, S., Coyle, T., Ryu, J. H., Yoon, W. H., and Park, D. S., 2011, "Optimization of Supersonic Nozzle Flow for Titanium Dioxide Thin-Film Coating by Aerosol Deposition," *J. Aerosol Sci.*, **42**(11), pp. 771–780.
- [10] Sova, A., Klinkov, S., Kosarev, V., Ryashin, N., and Smurov, I., 2013, "Preliminary Study on Deposition of Aluminium and Copper Powders by Cold Spray Micronozzle Using Helium," *Surf. Coatings Technol.*, **220**, pp. 98–101.
- [11] Sova, A., Smurov, I., Doubenskaia, M., and Petrovskiy, P., 2018, "Deposition of Aluminum Powder by Cold Spray Micronozzle," *Int. J. Adv. Manuf. Technol.*, **95**(9–12), pp. 3745–3752.
- [12] Akin, S., Wu, P., Tsai, J.-T., Nath, C., Chen, J., and Jun, M. B.-G., 2021, "A Study on Droplets Dispersion and Deposition Characteristics under Supersonic Spray Flow for Nanomaterial Coating Applications," *Surf. Coatings*

- Technol., **426**, p. 127788.
- [13] ANSYS Fluent 12.1 user guide, 2011, “No Title.”
- [14] Jen, T. C., Li, L., Cui, W., Chen, Q., and Zhang, X., 2005, “Numerical Investigations on Cold Gas Dynamic Spray Process with Nano- and Microsize Particles,” *Int. J. Heat Mass Transf.*, **48**(21–22), pp. 4384–4396.
- [15] Yin, S., Meyer, M., Li, W., Liao, H., and Lupoi, R., 2016, “Gas Flow, Particle Acceleration, and Heat Transfer in Cold Spray: A Review,” *J. Therm. Spray Technol.*, **25**(5), pp. 874–896.
- [16] Tsai, J.-T., Akin, S., Zhou, F., Bahr, D. F., and Jun, M. B.-G., 2021, “Establishing a Cold Spray Particle Deposition Window on Polymer Substrate,” *J. Therm. Spray Technol.*, pp. 1–12.
- [17] Özdemir, O. Ç., Conahan, J. M., and Müftü, S., 2020, “Particle Velocimetry, Cfd, and the Role of Particle Sphericity in Cold Spray,” *Coatings*, **10**(12), pp. 1–26.
- [18] Sova, A., Smurov, I., Doubenskaia, M., and Petrovskiy, P., 2018, “Deposition of Aluminum Powder by Cold Spray Micronozzle,” *Int. J. Adv. Manuf. Technol.*, **95**(9–12), pp. 3745–3752.
- [19] Schmidt, T., Assadi, H., Gärtner, F., Richter, H., Stoltenhoff, T., Kreye, H., and Klassen, T., 2009, “From Particle Acceleration to Impact and Bonding in Cold Spraying,” *J. Therm. Spray Technol.*, **18**(5–6), pp. 794–808.
- [20] Papyrin, A., Kosarev, V., Klinkov, S., Alkhimov, A., and Fomin, V. M., 2007, *Cold Spray Technology*, Elsevier Ltd.

- [21] “VixOne™ Nebulizers | Westmed, Inc.” [Online]. Available: <https://westmedinc.com/vixone/>. [Accessed: 26-Jan-2021].
- [22] Pattison, J., Celotto, S., Khan, A., and O’Neill, W., 2008, “Standoff Distance and Bow Shock Phenomena in the Cold Spray Process,” *Surf. Coatings Technol.*, **202**(8), pp. 1443–1454.

ACKNOWLEDGEMENTS

The first author of this study, Semih Akin, gratefully acknowledges the scholarship support by the Republic of Turkey Ministry of National Education. Semih Akin also acknowledges the Ward. A. Lambert Fellowship at Purdue University.

DECLARATION OF COMPETING INTEREST

The authors declare no competing interests.

AUTHOR CONTRIBUTIONS

Semih Akin: concept, methodology, formal analysis, investigation, design, modeling, numerical simulations, experiments, characterization, data curation, writing manuscript; **Puyuan Wu:** PIV measurements; **Chandra Nath:** concept, supervision, review & editing; **Jun Chen:** PIV measurements, supervision, review & editing; **Martin Byung-Guk Jun:** concept, supervision, methodology, resources, review & editing. All authors commented on the paper.